



HAL
open science

Estimation and Modeling of the Full Well Capacity in Pinned Photodiode CMOS Image Sensors

Alice Pelamatti, Vincent Goiffon, Magali Estriebeau, Paola Cervantes, Pierre Magnan

► **To cite this version:**

Alice Pelamatti, Vincent Goiffon, Magali Estriebeau, Paola Cervantes, Pierre Magnan. Estimation and Modeling of the Full Well Capacity in Pinned Photodiode CMOS Image Sensors. IEEE Electron Device Letters, 2013, vol. 34, pp. 900-902. 10.1109/LED.2013.2260523 . hal-00854018

HAL Id: hal-00854018

<https://hal.science/hal-00854018>

Submitted on 26 Aug 2013

HAL is a multi-disciplinary open access archive for the deposit and dissemination of scientific research documents, whether they are published or not. The documents may come from teaching and research institutions in France or abroad, or from public or private research centers.

L'archive ouverte pluridisciplinaire **HAL**, est destinée au dépôt et à la diffusion de documents scientifiques de niveau recherche, publiés ou non, émanant des établissements d'enseignement et de recherche français ou étrangers, des laboratoires publics ou privés.



Open Archive Toulouse Archive Ouverte (OATAO)

OATAO is an open access repository that collects the work of Toulouse researchers and makes it freely available over the web where possible.

This is an author-deposited version published in: <http://oatao.univ-toulouse.fr/>
Eprints ID: 9226

To link to this article: DOI: 10.1109/LED.2013.2260523
URL: <http://dx.doi.org/10.1109/LED.2013.2260523>

To cite this version: Pelamatti, Alice and Goiffon, Vincent and Estribeau, Magali and Cervantes, Paola and Magnan, Pierre *Estimation and Modeling of the Full Well Capacity in Pinned Photodiode CMOS Image Sensors*. (2013) IEEE Electron Device Letters, vol. 34 (n° 7). pp. 900-902. ISSN 0741-3106

Any correspondence concerning this service should be sent to the repository administrator: staff-oatao@inp-toulouse.fr

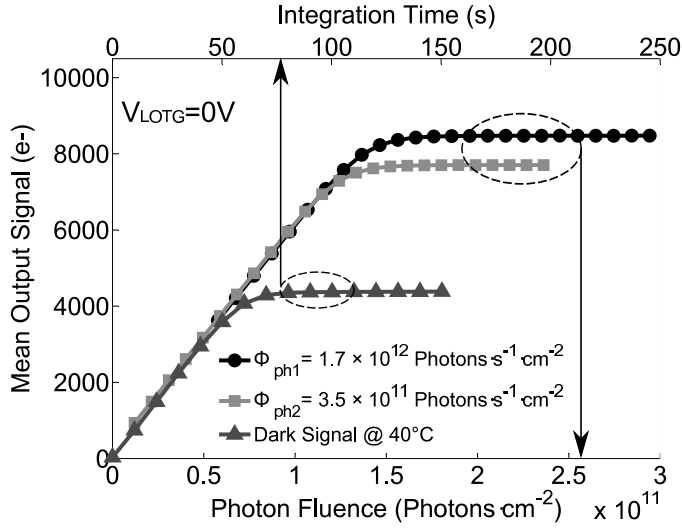


Fig. 2. Mean output signal measured for two constant photons fluxes Φ_{ph1} and Φ_{ph2} at increasing integration times. The figure also shows the evolution of the dark signal at 40°C (the discrepancy of the saturation level with the value measured at room temperature is less than 5%).

diode I-V curve (Fig. 3) at which the total current is null (open circuit condition). Fig. 1(b) shows a schematic of the equivalent circuit of the PPD plus the reset transistor when the FWC condition is reached. In our model we considered three main current contributions: the photocurrent $I_{ph} = \eta\Phi_{ph}$ (with η an efficiency factor < 1), the sub-threshold current I_{DS} of T_G , and the intrinsic forward current of the photodiode I_{fw} . At FWC condition, it yields:

$$I'_{D0} e^{\frac{V_{LOTG} - V_{FW} - V_T}{n v_{th}}} + I_{sat} \left(e^{-\frac{V_{FW}}{v_{th}}} - 1 \right) = \eta\Phi \quad (1)$$

where $I'_{D0} = I_{D0} \frac{W}{L}$, with I_{D0} a technological parameter and W and L respectively the width and the length of T_G . V_{FW} is the PPD voltage at full well, v_{th} is the thermal voltage, n is the strong inversion slope factor of the transistor (which for simplicity will be considered $n = 1$) and I_{sat} is the photodiode reverse current [5]. Generation and recombination processes within the depletion region of the PPD have been neglected. The Full Well Capacity Q_{FW} can be approximated as the product of C_{PPD} and the maximum voltage swing across the PPD ΔV_{PPDsat} , which, as shown in Fig. 3, can be estimated from the PPD pinning voltage V_{pin} [6] and the PPD saturation voltage V_{FW} :

$$Q_{FW} = -(V_{FW} - V_{pin}) \times C_{PPD} \quad (2)$$

where V_{FW} can be calculated from (1) as:

$$V_{FW} = -v_{th} \ln \left(\frac{\eta\Phi + I_{sat}}{I'_{D0} e^{\frac{V_{LOTG} - V_T}{v_{th}}} + I_{sat}} \right) \quad (3)$$

Note that even at low photon fluxes the photodiode is in the forward region, thus $V_{FW} > 0$. This implies that the maximum voltage swing across the PPD can be larger than the pinning voltage. The expression can be simplified for two biasing conditions depending on whether (a) T_G is accumulated (I_{DS}

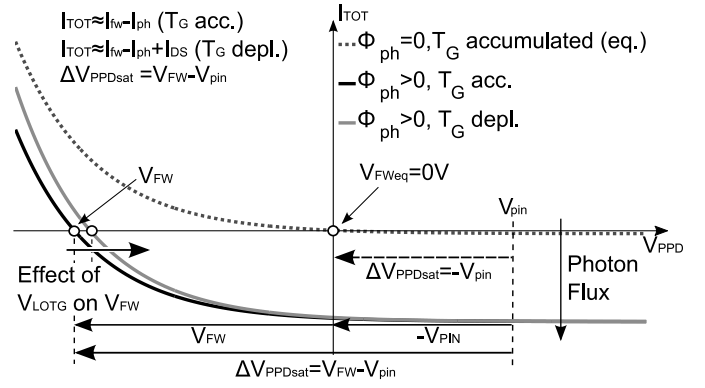


Fig. 3. Photodiode I-V characteristic (analytical model). The dotted line represents the characteristic at equilibrium (no photogeneration and no contribution of the transistor leakage current) while the solid black and grey represent the characteristic in light conditions with T_G respectively accumulated and depleted. The FW is reached when the total current is null, which corresponds to the open circuit condition V_{FW} . The maximum voltage swing across the photodiode is $\Delta V_{PPDsat} = V_{FW} - V_{pin}$. At equilibrium $V_{FW} = 0V$, thus $\Delta V_{PPDsat} = -V_{pin}$, which means that the pinning voltage can be estimated directly from the full well level at equilibrium.

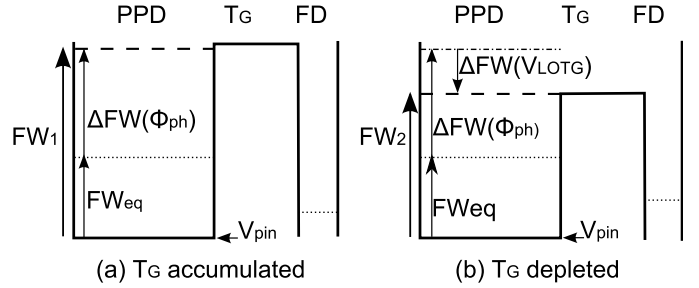


Fig. 4. Potential diagram of the PPD, T_G and FD structure illustrating the effect of the photon flux and V_{LOTG} potential on the PPD FWC for T_G accumulated (a) and depleted (b). FW_{eq} represents the Equilibrium FW level (no photo-generation and T_G accumulated), FW_1 is the FW level when the sensor is illuminated (photo-generation of excess carriers) and T_G is accumulated, while FW_2 is the FW level determined by the contribution of both the photo-generated excess carriers (which depends on the photon flux) and the transfer gate sub-threshold current.

can be neglected) or (b) T_G is depleted (the potential barrier between the PPD and the channel of T_G is lowered, with consequent contribution of the sub-threshold current I_{DS}):

$$Q_{FW}^a \approx \left[V_{pin} + v_{th} \ln \left(\frac{\eta\Phi_{ph} + I_{sat}}{I_{sat}} \right) \right] \times C_{PPD} \quad (4)$$

$$Q_{FW}^b \approx \left[V_{pin} - V_{LOTG} + V_T + v_{th} \ln \left(\frac{\eta\Phi_{ph}}{I'_{D0}} \right) \right] \times C_{PPD} \quad (5)$$

At the equilibrium (i.e. under no illumination and with T_G accumulated) the open circuit voltage V_{FW} is null, hence the maximum voltage swing across the photodiode directly gives an estimate of the pinning voltage. From this simple model we can easily infer the effects of the different parameters on the FWC depending on the biasing conditions of the transfer transistor. In the whole biasing range of V_{LOTG} , Q_{FW} depends logarithmically on the photon flux and has a linear dependence on V_{pin} and C_{PPD} . When T_G is depleted V_{LOTG} and V_T linearly affect the FWC by changing the height of the potential barrier between the photodiode and the transfer transistor channel, resulting in an electron flow from the PPD to the

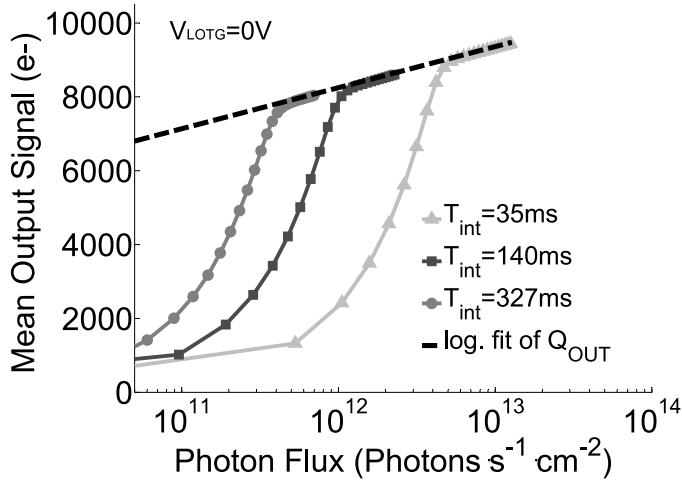


Fig. 5. Mean output signal measured for 3 constant integration times T_{int} at increasing photon flux. Since the FW level is increased by the increasing contribution of the photocurrent $I_{\text{ph}} = \eta\Phi_{\text{ph}}$, the curves never saturate. As it can be observed, the behavior of the FWC is well fitted by a logarithmic curve.

floating diffusion¹. The FWC dependence on the transistor parameters I_{D0} , W and L is logarithmic. To facilitate the understanding of the model, the effect of Φ_{ph} and V_{LOTG} on the potential distribution within the device during integration is schematized in Fig. 4.

III. EXPERIMENTAL VALIDATION

Fig. 5 shows the mean output signal as a function of the photon flux measured for three different integration times. As it can be observed, the curves never truly saturate since the FW level is continuously shifted because of the increasing photocurrent contribution (due to the increasing photon flux). As predicted, the FWC is well fitted by a logarithmic function. Fig. 6 shows the FWC (corresponding to the mean output signal (in e^-) Q_{out} determined in the saturation regime) as a function of the biasing voltage V_{LOTG} for two different photon fluxes. The results are once again consistent with the model, with a plateau when T_G is accumulated and a linear drop when T_G is depleted. The crossing from one operation mode to the other is indicated as V_{KneeTG} , which corresponds to the point at which the transistor leakage current is compensated by the diode forward current.

IV. CONCLUSION

A simple analytical model of the FWC of PPD CIS has been presented. This model is consistent with experimental data both under equilibrium (dark) condition, non-equilibrium (illuminated) condition and anti-blooming operating condition ($V_{\text{LOTG}} > V_{\text{KneeTG}}$), thus it can be very useful to identify the phenomenon limiting the FWC in a particular regime. The effect of the off-state biasing condition of the transfer transistor on the FWC has been shown and discussed. Note that the dependence on V_{LOTG} was also addressed in [1], [2], but no

¹The phenomenon attributed to a feedforward mechanism in [2] is included in the proposed model through the contribution of the T_G subthreshold current.

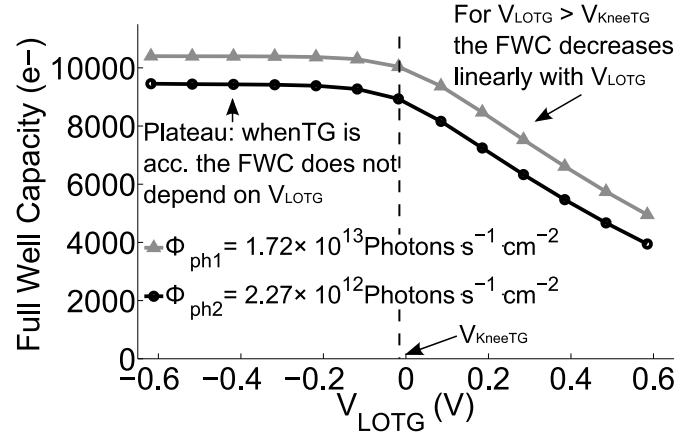


Fig. 6. FWC as a function of V_{LOTG} measured for two different photon fluxes. At $V_{\text{LOTG}} > V_{\text{KneeTG}}$ the FWC drops linearly with V_{LOTG} , while at $V_{\text{LOTG}} < V_{\text{KneeTG}}$ the FW level reaches a plateau. In both biasing conditions the photon flux level adds an offset to the FWC. The FWC value presented here corresponds to the mean output signal (in e^-) Q_{out} determined in the saturation regime (i.e. the saturation plateau in Fig. 2).

analytical model was proposed to support the experimental evidence. This letter has demonstrated that the FW level also strongly depends on the photon flux, showing that at classical illumination conditions the Full Well Capacity can be increased by a factor of 2 with respect to the value observed at equilibrium (the Equilibrium Full Well Capacity FWC_{eq}). This result is of primary importance for the characterization and the design of PPD CIS, since if the illumination level is not provided with a FWC value, large errors can be made in the evaluation of both the FWC and the parameters determined from the FWC. The proposed approach can be used as an alternative method to the one presented in [7] to evaluate the PPD pinning voltage. The FWC has been described in steady state illumination conditions. The extension of this model to the description of the transient behavior of the FWC (such as the one reported in [2]) will be discussed in a future work.

REFERENCES

- [1] B. Mheen, Y.-J. Song, and A. Theuwissen, "Negative offset operation of four-transistor CMOS image pixels for increased well capacity and suppressed dark current," *IEEE Electron Device Lett.*, vol. 29, no. 4, pp. 347–349, Apr. 2008.
- [2] M. Sarkar, B. Buttgen, and A. Theuwissen, "Feedforward effect in standard CMOS pinned photodiodes," *IEEE Trans. Electron Devices*, vol. 60, no. 3, pp. 1154–1161, Mar. 2013.
- [3] J. Bogaerts, G. Meynants, K. Van Wichelen, and E. Gillisjans, "Recent radiation testing on 180 nm and 110 nm CMOS image sensor processes," presented at *CNES Workshop on Radiation Effects on Optoelectronic Detectors*, Toulouse, Nov. 2012.
- [4] T. Watanabe, J.-H. Park, S. Aoyama, K. Isobe, and S. Kawahito, "Effects of negative-bias operation and optical stress on dark current in CMOS image sensors," *IEEE Trans. Electron Devices*, vol. 57, no. 7, pp. 1512–1518, Jul. 2010.
- [5] Y. Taur and T. H. Ning, *Fundamentals of Modern VLSI Devices*, 2nd ed. Cambridge University Press, Aug. 2009.
- [6] A. Krymski and K. Feklistov, "Estimates for scaling of pinned photodiodes," in *Proc. IEEE Workshop On CCD and Advanced Image Sensors*, Jun. 2005, pp. 60–63.
- [7] J. Tan, B. Buttgen, and A. Theuwissen, "Analyzing the radiation degradation of 4-transistor deep submicron technology CMOS image sensors," *IEEE Sensors J.*, vol. 12, no. 6, pp. 2278–2286, Jun. 2012.